CHAPTER 7

PEROVSKITE PHASE FORMATION AND FERRO-ELECTRIC PROPERTIES OF THE PNN–PZN–PZT TERNARY SYSTEM

Overview—The ternary system of lead nickel niobate $Pb(Ni_{1/3}Nb_{2/3})O_3$ (PNN), lead zinc niobate $Pb(Zn_{1/3}Nb_{2/3})O_3$ (PZN) and lead zirconate titanate $Pb(Zr_{1/2}Ti_{1/2})O_3$ (PZT), has been investigated to determine the influence of different solid state processing conditions on the dielectric and ferroelectric properties. The ceramic materials were characterized by means of X-ray diffraction (XRD), dielectric measurements, and hysteresis measurements. The phase-pure perovskite phase of PNN–PZN–PZT ceramics was obtained over a wide compositional range. It was observed that for the ternary system *0.5*PNN–*(0.5-x)*PZN–*x*PZT, the change in the transition temperature (T_m) is approximately linear with respect to the PZT content in the range $x = 0$ to 0.5. With an increase in x, T_m shifts up to high temperatures. Examination of the remanent polarization (P_r) revealed a significant increase with increasing x. In addition, the relative permittivity (ε_r) increased as a function of x. The highest permittivities (ε_r = 22,000) and the highest remanent polarization (P_r = 25 $\mu C/cm^2$) were recorded for the binary composition *0.5*$Pb(Ni_{1/3}Nb_{2/3})O_3$–*0.5*$Pb(Zr_{1/2}Ti_{1/2})O_3$.

7.1 Introduction

Lead-based complex perovskites, such as $Pb(Zn_{1/3}Nb_{2/3})O_3$ (PZN) and $Pb(Ni_{1/3}Nb_{2/3})O_3$ (PNN), having the general formula $Pb(B'B'')O_3$ have received significant attention since 1970's because of their peculiar dielectric and piezoelectric behavior.[26,47] These materials have been applied in many areas such as electrostrictive actuators, transducers, and multilayer ceramic capacitors (MLCCs).[6,13]

Lead zinc niobate, PZN, was first synthesized in the 1960s.[47] Its permittivity versus temperature curve displayed a broad peak around 140°C (T_m) with a strong frequency dependence. Extremely high relative permittivity has been measured in the vicinity of the peak with a $\varepsilon_r \sim 60{,}000$ reported for single crystals.[25] Nanometer-level chemical heterogeneity in the form of short range order of Zn^{2+} and Nb^{5+} at B-sites was proposed to account for the observed diffuse phase transition.[10,56] The crystal structure of PZN is rhombohedral (*3m*) at room temperature and transforms to cubic (*Pm3m*) at high temperatures.[25]

Unfortunately, phase-pure perovskite PZN polycrystalline ceramics have not been synthesized by conventional solid state reaction methods because of a steric and an electrostatic interaction between high polarization of Pb^{2+} cation and the Zn^{2+} cation which favor the formation of the pyrochlore phase instead of the perovskite phase.[71] Moreover, the low tolerance factor and small electronegativity difference[16] makes the perovskite phase unstable requiring the addition of normal ferroelectric compounds such as $BaTiO_3$[28] and $PbTiO_3$[27] to stabilize the perovskite phase.

Recently Fan and Kim[24] mixed $Pb(Zr_{0.47}Ti_{0.53})O_3$ with PZN by a conventional solid-state reaction method and successfully stabilized perovskite PZN.

A morphotropic phase boundary (MPB) between the PZN-rich rhombohedral phase and the PZT-rich tetragonal phase was reported at PZN:PZT(47/53) = 1:1. At this composition, a high electromechanical coupling factor of k_p= 0.67 was measured.

Lead nickel niobate, PNN, exhibits a diffuse phase transition around -120°C with a much lower peak permittivity of about 4000.[40] The crystal structure of PNN at room temperature is cubic (*Pm3m*) with a lattice parameter of 4.03 Å.[40] Phase-pure perovskite PNN can be prepared via the columbite method.[41] Luff *et al*[43] investigated solid solutions in the PNN–$PbTiO_3$–$PbZrO_3$ system and identified the composition of *0.5*PNN–*0.35*PT–*0.15*PZ with optimal piezoelectric properties. Detailed reaction kinetics during solid state processing of PNN–PZT was recently investigated by Babushkin[64] and several pyrochlore phases have been detected. The piezoelectric PNN–PZT ceramics have found wide applications and are now commercially available.

The investigation of the ferroelectric properties of the PNN–PZN–PZT ternary system is of interest for a number of reasons. Both PNN and PZN have distinct transition temperatures and the transition temperature for the solid solution of PNN–PZN should lie in the ambient temperature range. This implies that the ultrahigh permittivity values can be realized at room temperature. As demonstrated in the binary PZN–PZT and PNN–PZT systems, the addition of PZT imparts superior piezoelectric properties to the solid solutions. Therefore, there is great potential for excellent dielectric and piezoelectric properties within the ternary system PNN–PZN–PZT.

Information in the literature on the PNN–PZN–PZT ternary system is extremely limited. Lee *et al*[72] tried to fabricate phase-pure perovskite PNN–PZN–

PZT ceramics with a Zr/Ti ratio in PZT of 1.0. In their study, powders of PZT, PZN, and PNN were prepared separately and then mixed and calcined again to form perovskite PNN–PZN–PZT. The highest amount of perovskite phase in their work was found to be 92%.[72] The Curie temperature was found to vary form 50 to 250°C, depending on the mole fraction of PZT. The best piezoelectric properties at room temperature, k_p = 0.63, were found in the composition *0.5*PNN–*0.3*PZN–*0.2*PZT.[72]

The presence of pyrochlore phase is extremely detrimental to the dielectric and piezoelectric properties in most perovskite ceramics. The process of pre-reacting the B-site cations to form a columbite phase $B'B''_2O_6$ prior to the addition of PbO has been successfully applied to many systems to suppress pyrochlore phase formation.[16,41] However, this technique has been largely unsuccessful for PZN and fabrication of phase-pure PZN-containing solid solutions remains a challenging issue. A processing route different from that used previously by Lee *et al.*[72] was used to successfully prepare phase-pure perovskite PNN–PZN–PZT ceramics. The use of the double crucible technique, using excess PbO, and maintaining a fast heating rate were all found to be essential factors in perovskite phase development.

7.2 Experimental procedure

In this method, the columbite precursors $ZnNb_2O_6$ and $NiNb_2O_6$ were prepared from the reaction between ZnO (99.9%) and Nb_2O_5 (99.9%) at 975°C for 4 hours and between NiO (99.9%) and Nb_2O_5 (99.9%) for 4 hours at 1100°C, respectively. The wolframite phase $ZrTiO_4$ was formed by reacting ZrO_2 (99.9%) with TiO_2(99.9%) at 1400°C for 4 hours. The powders of $ZnNb_2O_6$, $NiNb_2O_6$, and $ZrTiO_4$ were mixed in the required stoichiometric amounts with PbO (99.9%) with an excess

of 2 mol% of PbO added. The compositions synthesized in this study were $x = 0, 0.1, 0.3,$ and 0.5 in the ternary system 0.5PNN–$(0.5-x)$PZN–xPZT. The milling process was carried out for 24 hours in isopropyl alcohol. After drying at 120°C the powders were calcined at 900°C-950°C for 4 hours in a double crucible configuration with a heating rate of 20°C/min. After grinding and sieving, 5 wt% of polyvinyl alcohol (PVA) binder was added. Discs with a diameter of 1.5 cm were prepared by cold uniaxial pressing at a pressure of 150 MPa. Binder burnout occurred by slow heating to 500°C and holding for 2 hours. To investigate the sintering behavior, the discs were sintered in a sealed alumina crucible at temperatures ranging from 950°C-1250°C using a heating rate of 5°C/min and a dwell time of 2 hours. Phase formation and crystal structure of the calcined powders and sintered discs were examined by XRD. Data collection was performed in the 2θ range of 20°– 60° using step scanning with a step size of 0.02° and counting time of 2s/step.

The relative amounts of perovskite and pyrochlore phase were determined by measuring the primary X-ray peak intensities of the perovskite and pyrochlore phase. The percentage of perovskite phase was estimated by the following equation (3.1) The pellets were polished and electroded via gold sputtering, over which a layer of air-dried silver paint was applied. The relative permittivity (ε_r) and dissipation factor ($\tan\delta$) of the pellets sample were measured at various temperatures ranging from -100°C to 180°C with a heating and cooling rate of 3°C/min over the frequency range between 100 Hz to 100 kHz using an LCR meter (HP 4284A) in conjunction with a Delta Design 9023 temperature chamber. The remanent polarization P_r was determined from a P–E hysteresis loop measurements using a Sawyer-Tower circuit at temperatures between -66°C and 60°C.

7.3 Results and discussion

7.3.1 Perovskite phase development

The perovskite and pyrochlore phase formation at different calcination temperatures in *0.5*PNN–*(0.5-x)*PZN–*x*PZT powders with *x = 0.1-0.5* were studied and analyzed by XRD. X-ray diffraction patterns from this system are given in Fig. 7.1. The cubic pyrochlore-type structure of $Pb_{1.83}(Nb_{1.71}Zn_{0.29})O_{6.39}$ (JCPDS No. 25-0446) was identified in the *x = 0.0*, *0.1* and *0.3* compositions at the 900°C calcination temperature.

The pyrochlore formation reaction from PbO and the columbite precursors is an extremely fast process which is completed within 2-3 min at temperatures as low as 750°C.[73] With increased calcination temperatures the amount of perovskite phase increased sharply. In this work it was observed that the primary phase in all of the compositions at 950°C was well-crystallized perovskite. Within the detection limits of the XRD technique, the samples were essentially 100% perovskite and free of pyrochlore. The heat treatment and percent perovskite phase for all the compositions are listed in Table 7.1. The first two rows listed are for the calcined powders, and the remaining data are derived from sintered samples using powders calcined at 950°C. In this study, the combination of using a double crucible, excess PbO (2 mol%), and a fast heating/cooling rate (20°C/min) were shown to be effective in reducing the total amount of pyrochlore phase during calcination at 950°C. The 2 mol% excess PbO was chosen because there have been observations reported that compositions with excess PbO additions greater than 2.8 mol% resulted in degraded electrical properties. This was attributed to the presence of an excess PbO layer at the grain boundary.[74,75]

XRD patterns from a set of samples prepared at various sintering temperatures are given in Fig. 7.2. In this study, for the $x = 0$ composition single-phase perovskite was obtained for sintering temperatures below 1150°C. Above 1150°C, the cubic pyrochlore phase $Pb_{1.83}(Nb_{1.71}Zn_{0.29})O_{6.39}$ (JCPDS No. 25-0446) formed and the percentage of pyrochlore phase increased as the sintering temperature increased, as shown in Table 7.1. This behavior also appeared in the $x = 0.1$ composition at sintering temperatures above 1200°C. The behavior is believed to be due to the volatilization of PbO at high temperatures. Nevertheless, the XRD patterns for the $x = 0.3$ and $x = 0.5$ compositions do not show the formation of the pyrochlore phase. It is interesting to note that the intensity of (100) perovskite peak decreased at high temperatures for the $0.1 \leq x \leq 0.5$ composition.

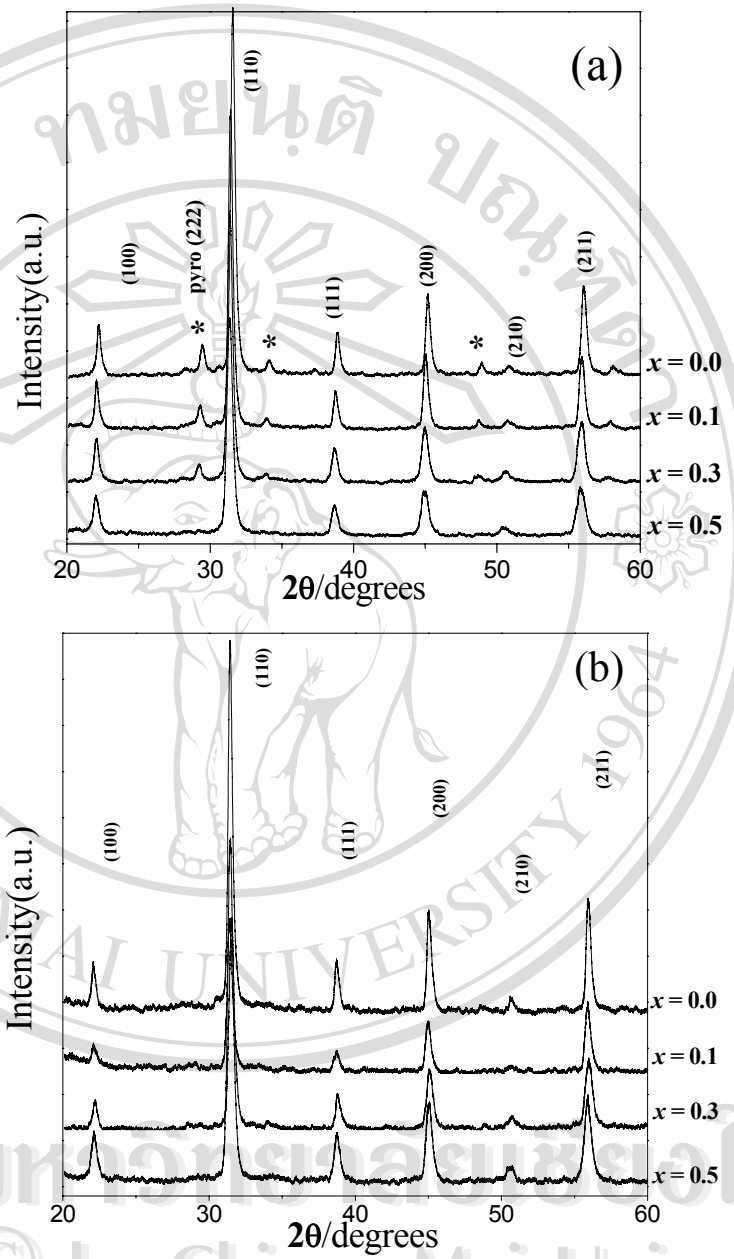

Figure 7.1 Powder XRD patterns of a stoichiometric composition of *0.5*PNN–*(0.5-x)* PZN–*x*PZT ceramics: (a) Calcined at 900°C for 4h with 20°C/min heating rate; (b) Calcined at 950°C for 2h with 20°C/min heating rate. Pyrochlore phase indicated with *.

Table 7.1 Perovskite phase development during calcinations and sintering process of *0.5*PNN–*(0.5-x)*PZN–*x*PZT system (The first two rows indicate the data in calcined powders and the rest rows are data from sintering of powders calcined at 950°C).

Temperature (°C)	Perovskite Phase (%)			
	x = 0.0	*x = 0.1*	*x = 0.3*	*x = 0.5*
900*	91.53	92.67	92.5	100
950*	100	100	100	100
1000	100	100	-	-
1050	100	100	100	-
1100	100	100	100	-
1150	100	100	100	100
1200	84.468	100	100	100
1225	76.249	76.79	100	100
1250	-	-	100	100
1275	-	-	100	100

* calcination temperature

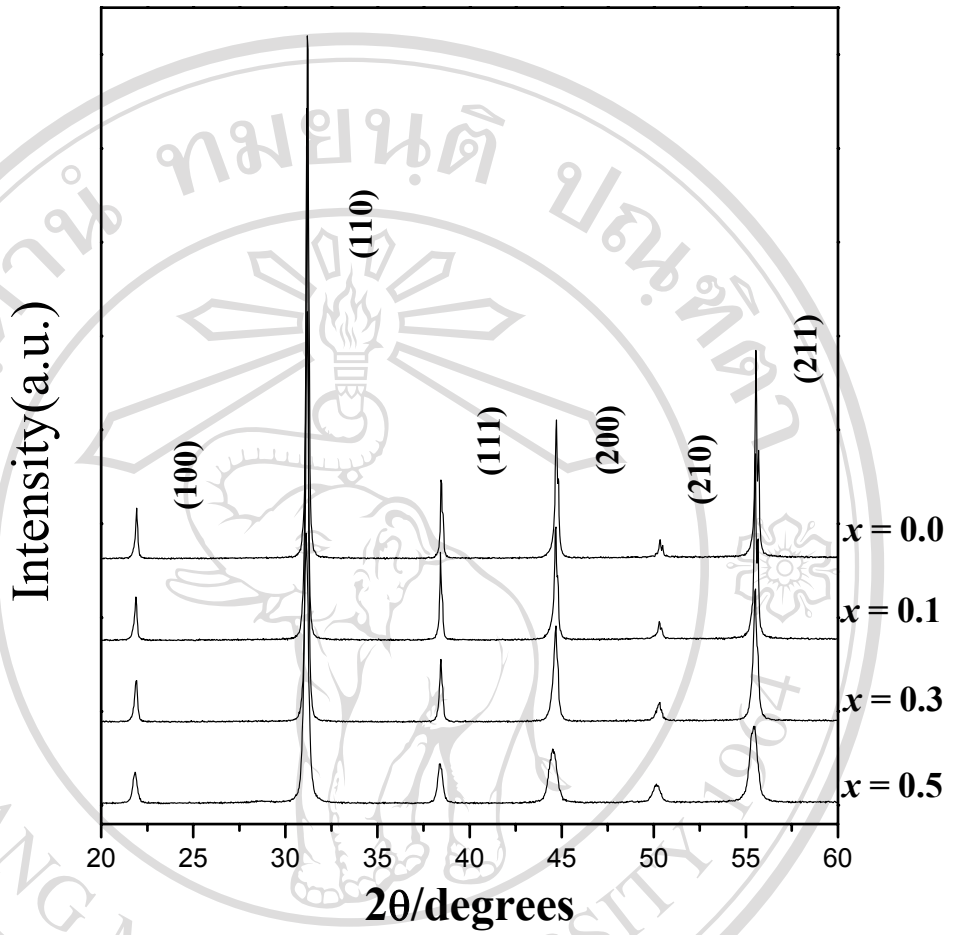

Figure 7.2 XRD patterns of *0.5*PNN–*(0.5-x)*PZN–*x*PZT ceramics at the optimum sintering conditions.

In the PNN–PZN–PZT system, the A-site is occupied by Pb^{2+} (1.630Å) ions, and the Ni^{2+}, Nb^{5+}, Zn^{2+}, Zr^{4+}, and Ti^{4+} ions occupy the B site of the ABO_3 perovskite crystal structure. The average ionic radius of B-site ions in the composition $0.5Pb(Ni_{1/3}Nb_{2/3})O_3$–$(0.5-x)Pb(Zn_{1/3}Nb_{2/3})O_3$–$xPb(Zr_{1/2}Ti_{1/2})O_3$ can be calculated from the following equation:

$$r_{B-site} = 0.5\left[\tfrac{1}{3} r_{Ni^{2+}} + \tfrac{2}{3} r_{Nb^{5+}}\right] + (0.5 - x)\left[\tfrac{1}{3} r_{Zn^{2+}} + \tfrac{2}{3} r_{Nb^{5+}}\right] + x\left[\tfrac{1}{2} r_{Zr^{4+}} + \tfrac{1}{2} r_{Ti^{4+}}\right] \quad (7.1)$$

where the ionic radii of Ni^{2+}, Nb^{5+}, Zn^{2+}, Zr^{4+}, and Ti^{4+} are 0.830, 0.780, 0.880, 0.860 and 0.745 Å, respectively.[17] Using simple description of the geometric packing within perovskite structure, mentioned in section 1.3.3. The calculated average B-site ionic radii and tolerance factor of the PNN–PZN–PZT system is presented in Table 7.2 using 1.260 Å for the radius of O^{2-}.[17] The effective size of the B-site ion decreases with an increasing mole faction of PZT primarily due to the smaller ionic radii of Ti^{4+}. This results in a slight increase in the tolerance factor as it approaches 1.0. However, the lattice parameter is found to increase as the mole faction of PZT increases, and the symmetry changes from pseudo-cubic to rhombohedral.

The crystal symmetry of PNN at room temperature was determined to be pseudo-cubic perovskite with a cell parameter a = 4.0308 Å. The PZN composition at room temperature was determined to be the rhombohedral space group *R3m*. According to the $PbZrO_3$–$PbTiO_3$ phase diagram, at room temperature $Pb(Zr_{1/2}Ti_{1/2})O_3$ is within the tetragonal phase field near the MPB region.[13]

In this work, the crystal structure and lattice parameters of the PNN–PZN–PZT compositions were determined through room temperature diffraction experiments. The indexing procedure of the perovskite phase in the $x = 0.0$ and $x = 0.1$ samples was performed based on cubic symmetry. For the $x = 0.3$ and 0.5 samples, however, no splitting of 002 and 200 peak was observed with increased PZT concentration, as shown in Fig. 7.2. However, the superposition was clearly observed for the (220) peak as shown in Fig. 7.3. This result indicates that the crystal structure was rhombohedral. In addition, from the data listed in Table 7.2 it is evident that the lattice parameter a increased with increasing concentration of PZT due to the increase in B-site radius.

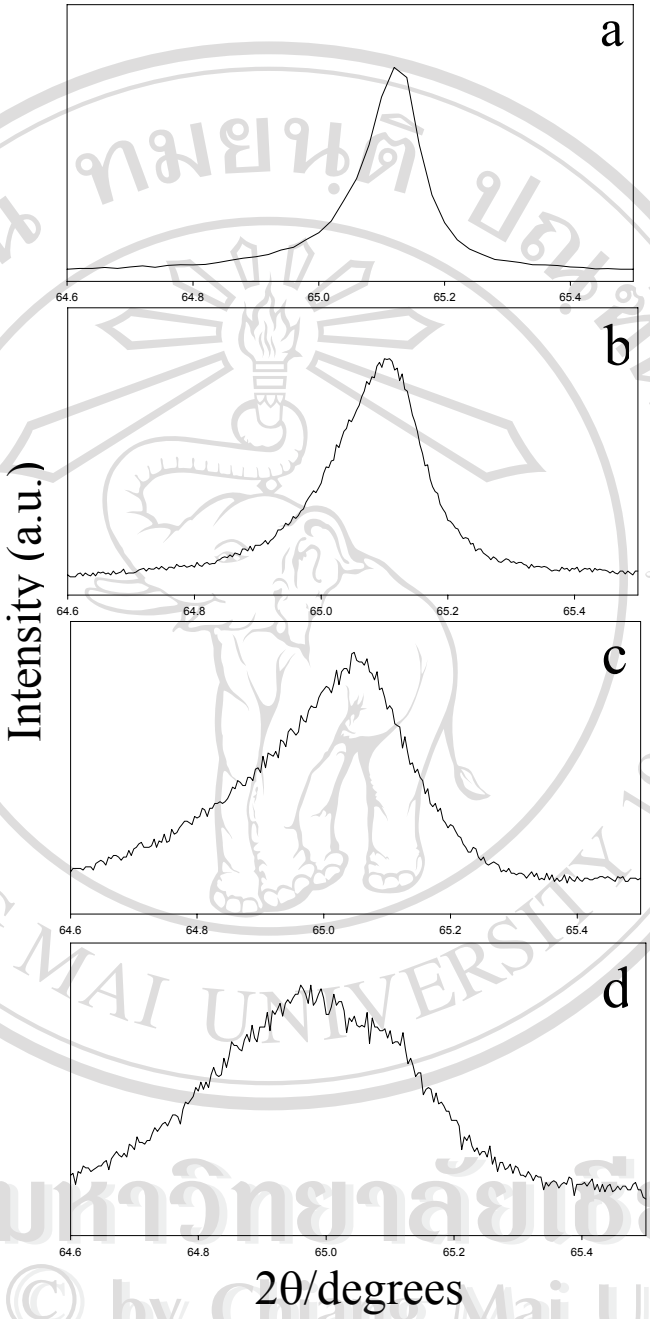

Figure 7.3 XRD patterns of the (220) peak of *0.5*PNN-(*1-x*)PZN- *x* PZT ceramic ; a : *x = 0* , b: *x = 0.1*, c: *x = 0.3*, d: *x = 0.5* .

Table 7.2 Comparison of the calculated average B-site ionic radii, the crystal structure, and lattice parameters derived from XRD data.

Composition *0.5*PNN–*(0.5-x)*PZN–*x*PZT	Average B-site ionic radii (Å)	tolerance factor, *t*	Lattice parameter, *a* (Å)	Crystal structure	Distortion angle, α
x = 0.0	0.704	0.881	4.049	Cubic	90.0
x = 0.1	0.707	0.880	4.054	Cubic	90.0
x = 0.3	0.712	0.878	4.057	Rhombohedral	89.88
x = 0.5	0.718	0.875	4.060	Rhombohedral	89.89

7.3.2 Dielectric properties

The permittivity at 1 kHz as a function of temperature for *0.5*PNN–*(0.5-x)*PZN–*x*PZT ceramics under different sintering conditions is shown in Fig. 7.4. The sintering temperature was found to have a significant effect on the permittivity. All compositions exhibited an increase in the permittivity with increased sintering temperatures. However, at the highest sintering temperature the permittivity decreased due to the formation of a pyrochlore phase. The *x = 0* composition showed an increase in permittivity up to a maximum of 10,000 at a sintering temperature of 1150°C. At higher sintering temperatures there is both a decrease in permittivity and a shift in the temperature at which the permittivity is maximum (T_m) from -20 to -50°C. This shift in T_m is likely to be the result of a change in the stoichiometry of the perovskite phase due to the effects of Zn volatilization and the formation of the pyrochlore phase $Pb_{1.83}(Nb_{1.71}Zn_{0.29})O_{6.39}$. This shifted the overall perovskite composition closer to PNN, with a lower T_m of –120°C. In addition, the decrease in permittivity that was observed was the result of the low permittivity of $Pb_{1.83}(Nb_{1.71}Zn_{0.29})O_{6.39}$ ($\varepsilon_r \sim 100$).

The *x = 0.1* composition exhibited a maximum permittivity of approximately 12,000 with a $T_m \sim 0^oC$ at a sintering temperature of 1200°C. Higher sintering temperatures resulted in a decrease in the permittivity. Likewise the *x = 0.3* composition exhibited a maximum permittivity of 17,000 at $T_m = 70\ ^oC$ at a sintering temperature of 1200°C. Consistent with the other compositions, increased sintering temperatures resulted in a decrease in permittivity and a shift in T_m. Finally, the highest permittivities in this study were recorded for the *x = 0.5* composition at a sintering temperature of 1250°C with $\varepsilon_{r,max} = 22,000$ at $T_m \sim 120^oC$. This is

significantly larger than the previous value reported in the literature. In this work the dielectric experiments showed that the optimum sintering conditions for *0.5*PNN–*(0.5-x)*PZN–*x*PZT were the temperature of at 1150°C, 1200°C, 1200°C, and 1250°C, for the $x = 0$, $x = 0.1$, $x = 0.3$, and $x = 0.5$ compositions, respectively, with a dwell time of 2 hours. Ceramics sintered under these conditions were used in the determination of the crystal structure and lattice parameters, which had been shown in Figs. 7.2 and 7.3, and Table 7.2. The following characterization of the dielectric and ferroelectric properties of each composition was also carried out in sample sintered at their optimum conditions.

Fig. 7.5 shows the dielectric properties for each composition at the optimum sintering conditions. All of compositions showed a broadening of the permittivity maxima and the T_m increased with increasing measurement frequency, as expected. Experimental results indicate that all of compositions show a diffuse phase transition with the strong frequency dispersion which is characteristic of relaxor ferroelectrics.[76]

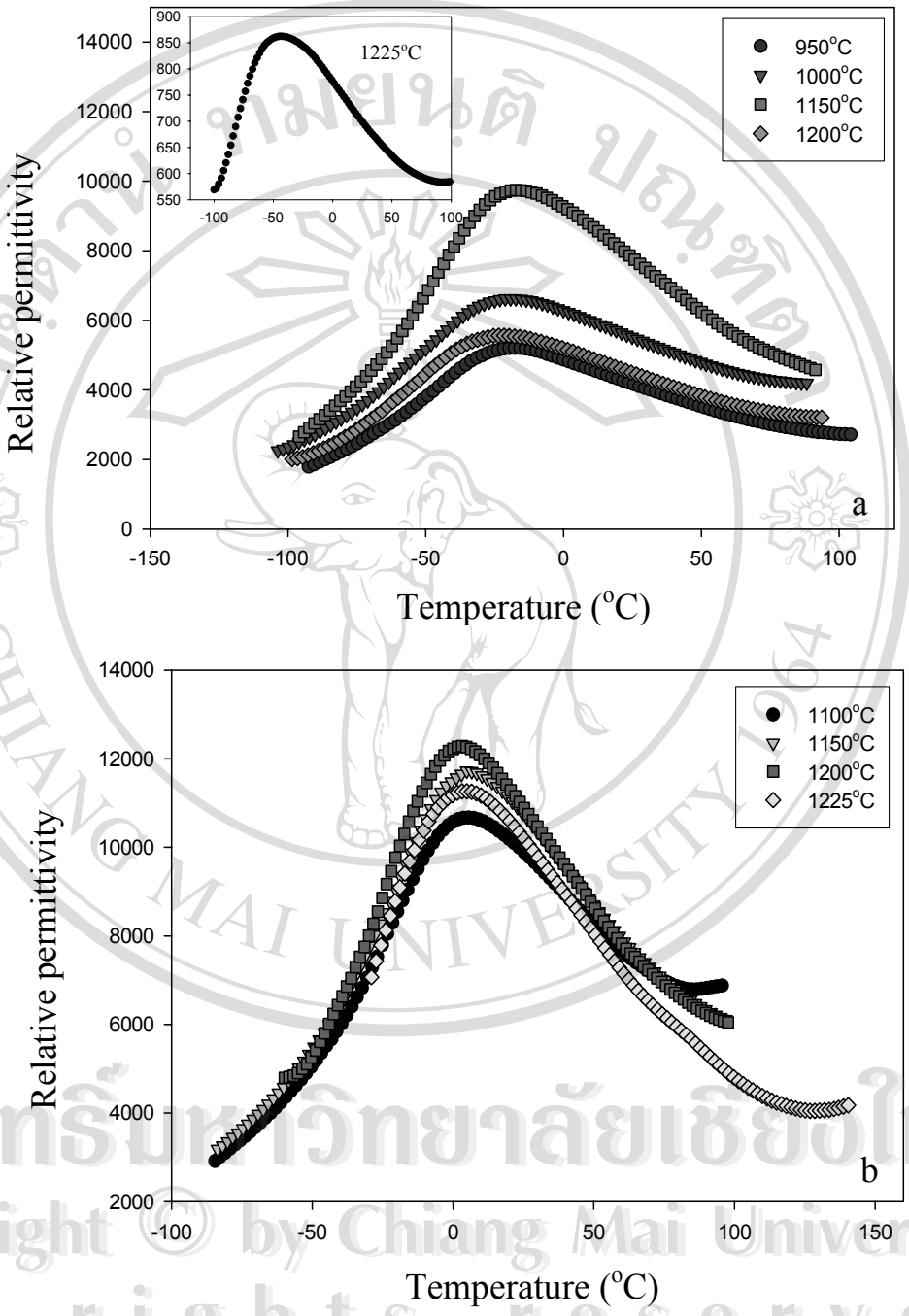

Figure 7.4 Relative permittivity and dissipation factor at 1kHz for *0.5*PNN-(*0.5-x*)PZN- *x*PZT ; a : *x = 0*, b : *x = 0.1*. Dielectric data for difference sintering temperature is shown.

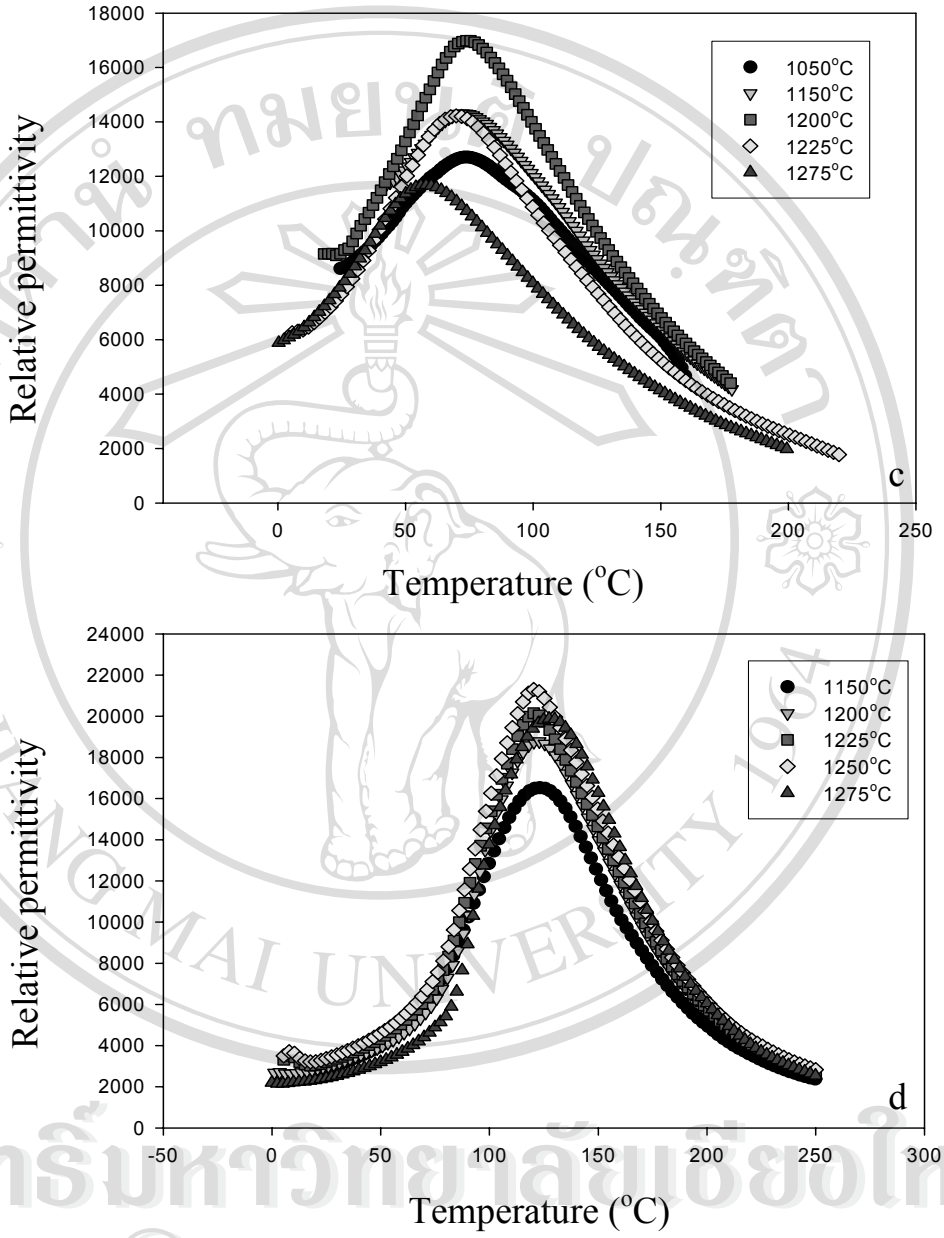

Figure 7.4 Relative permittivity and dissipation factor at 1kHz for *0.5*PNN-(*0.5-x*)PZN- *x*PZT ; c : *x = 0.3* ,d : *x = 0.5*. Dielectric data for difference sintering temperature is shown.

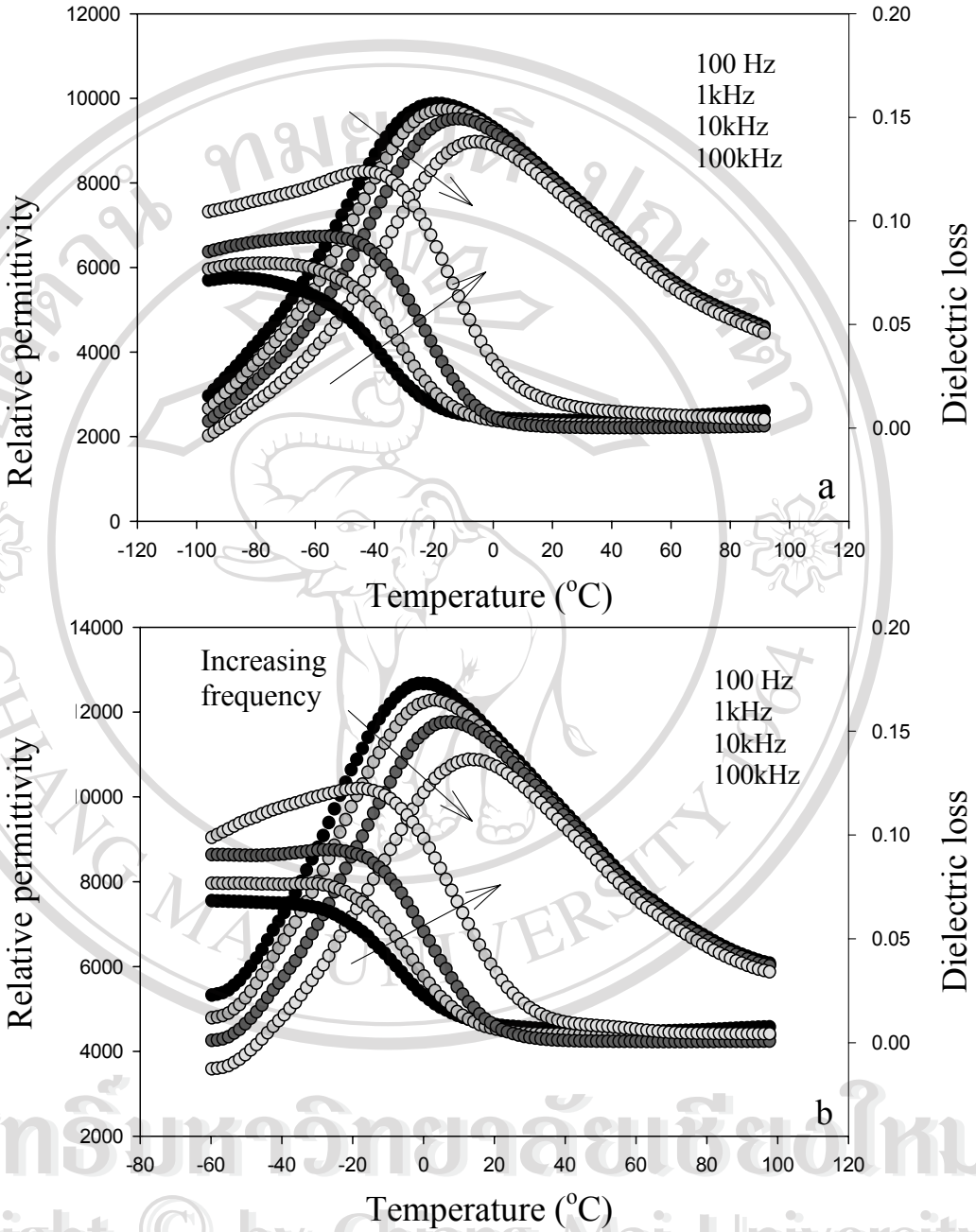

Figure 7.5 Relative permittivity and dissipation factor of *0.5*PNN–*(0.5-x)*PZN–*x*PZT ceramics prepared at the optimum sintering conditions.

a: $x = 0$, ceramics sintered at 1150°C for 2h;

b: $x = 0.1$, ceramics sintered at 1200°C for 2h;

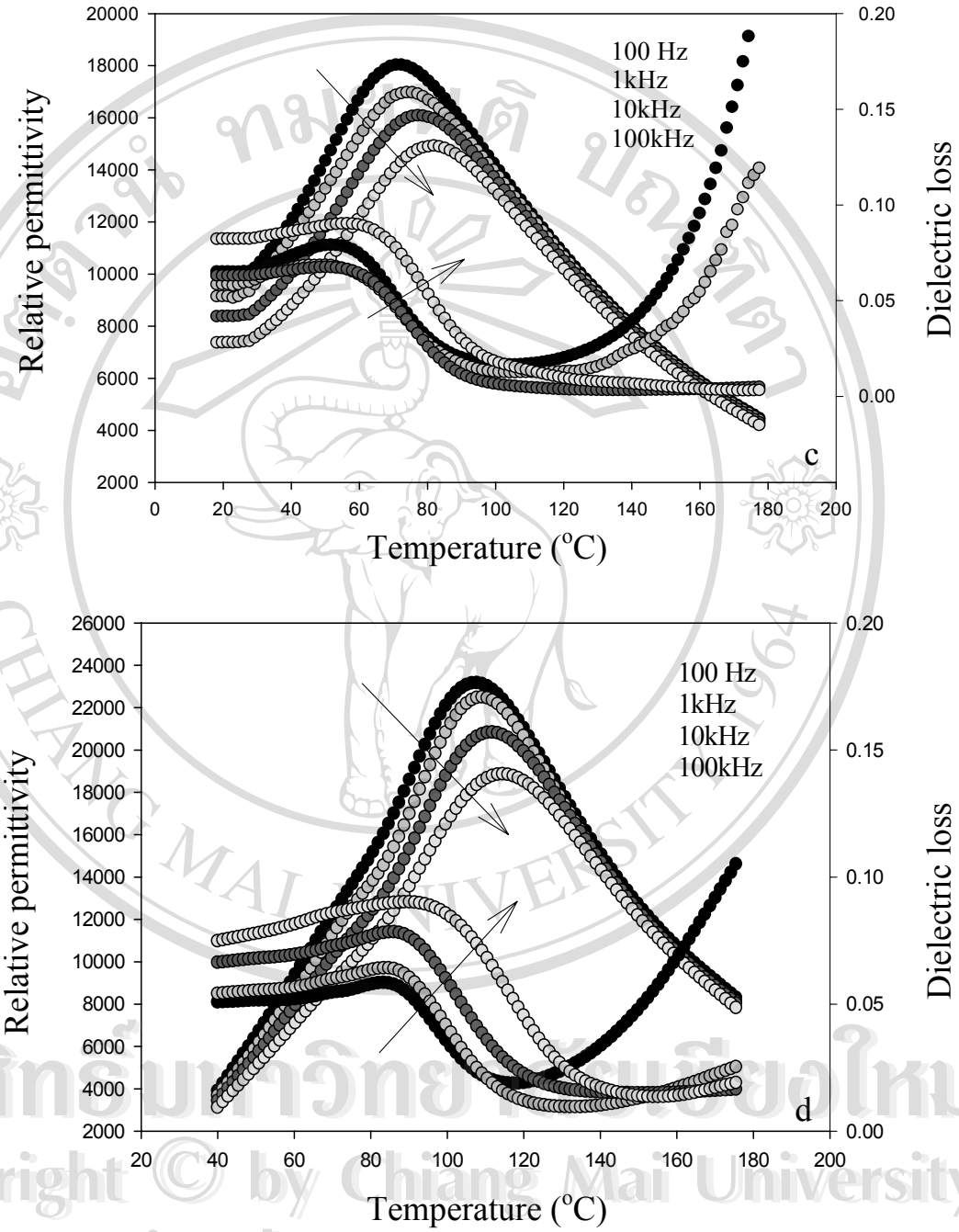

Figure 7.5 Relative permittivity and dissipation factor of *0.5*PNN–*(0.5-x)*PZN–*x*PZT ceramics prepared at the optimum sintering conditions.

c: $x = 0.3$, ceramics sintered at 1200°C for 2h;

d: $x = 0.5$, ceramics sintered at 1250°C for 2h.

Table 7.3 Comparisons of dielectric properties of ceramics in the *0.5*PNN–*(0.5-x)*PZN–*x*PZT system at the optimum sintering conditions.

	Composition *0.5*PNN–*(0.5-x)*PZN–*x*PZT	Percent perovskite	T_m (°C)	Relative permittivity (at 25°C) at 1 kHz	Relative permittivity (at T_m) at 1 kHz	Dielectric loss (at 25°C) at 1 kHz
Lee *et al*. [72]	*x = 0.0*	85	55	4000	6000	-
	x = 0.1	87	80	4700	8000	-
	x = 0.3	92	140	5500	13000	-
	x = 0.5	78	225	2500	7000	-
Vierheilig *et al*. [35]	*x = 0.0*	100	-10	6077	6980	0.010
This work	*x = 0.0*	100	-20	8500	9700	0.011
	x = 0.1	100	0	11500	13000	0.032
	x = 0.3	100	70	9000	18000	0.050
	x = 0.5	100	125	4000	22000	0.048

From this result, it is clear from the sharpness of the permittivity peak that the compositions gradually approached normal ferroelectric behavior as the mole fraction of PZT increased. As *x* approached 0, the behavior was strongly relaxor in nature. This may be a function of the degree of B-site cation ordering or the influence of the macro-domains.

In general, the sintering temperature of this system increased with increased mole percent of PZT. Both the maximum permittivity $\varepsilon_{r,max}$ and T_m increased quasi-linearly as the molar fraction of PZT increased. The T_m of the constituent compounds PNN, PZN, and PZT are -120°C, 140°C, and 390°C, respectively, which can be used to calculate an empirical estimate of T_m via the equation:

$$T_m = 0.5 \times (-120^o C) + (0.5 - x) \times (140^o C) + x \times (390^o C) \qquad (7.2)$$

The variation of the measured T_m, the calculated T_m, and the measured $\varepsilon_{r,max}$ with composition *x* is shown in Fig. 7.6. It is evident that Equation (7.2) gives a reasonable indication of the transition temperature T_m. A summary of the dielectric properties for each of the compositions is shown in Table 7.3. As Table 7.3 illustrates, the PNN–PZN–PZT ceramics in this study resulted in significantly higher permittivity than in previous studies. Through controlling PbO loss and preventing pyrochlore phase formation, single-phase perovskite ceramics can be processed with excellent electrical properties.

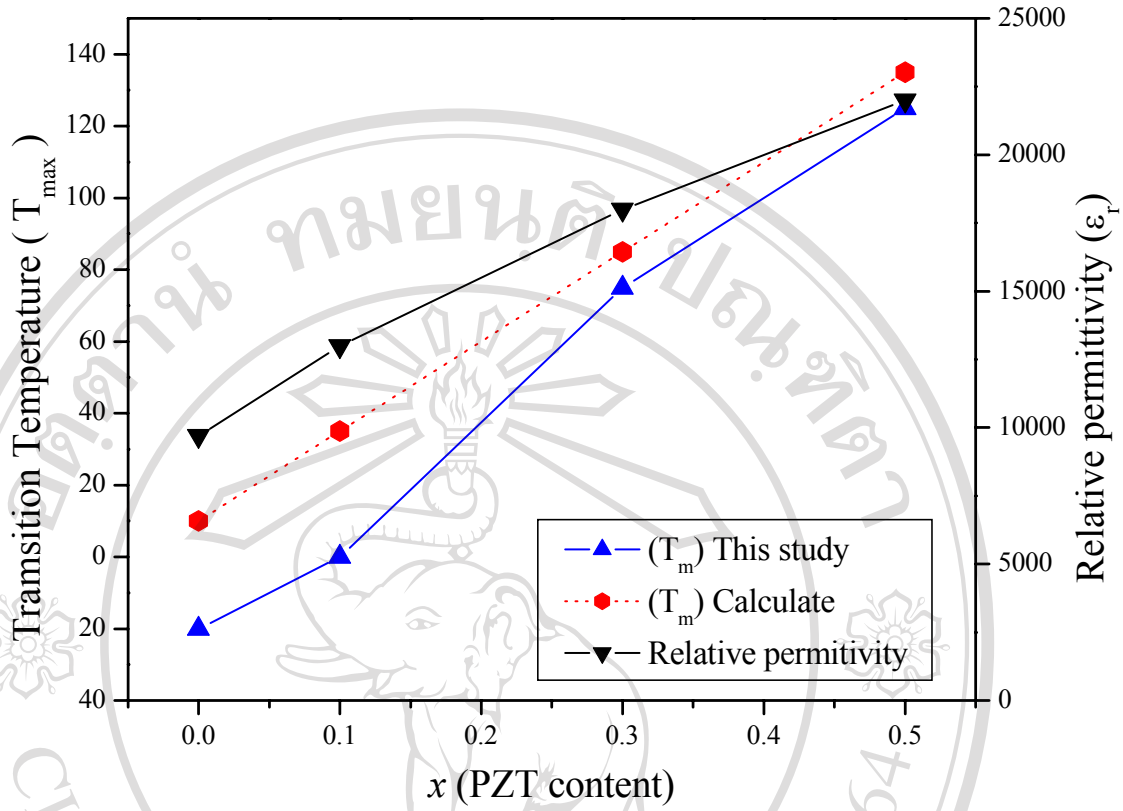

Figure 7.6 T_m, Calculated T_m and room temperature relative permittivity as a function of composition *x* at 1 kHz.

7.3.3 Ferroelectric and Electrostictive properties

Polarization hysteresis measurements at room temperature were performed using a modified sawyer-tower circuit. The hysteresis loops as a function of *x* are shown in Fig 7.7. The *x = 0* and *x = 0.1* compositions exhibited slim loops characteristic of relaxor ferroelectrics. The saturation polarization P_s, remanent polarization P_r, and coercive field E_c were increased with increased mole percent of PZT as illustrated in Table 7.4. The loop area values were calculated by integrating the polarization with respect to the electric field. The maximum remanent polarization was observed for the *x = 0.5* composition. The values of P_s, P_r and E_c for

the $x = 0.5$ composition are 31.9 μC/cm^2, 25.2 μC/cm^2, and 4.0 kV/cm, respectively. These hysteresis data are consistent with the dielectric results in illustrating the gradual trend from relaxor to normal ferroelectric as the mole fraction of PZT is increased.[77] The hysteresis loops for the compositions $x = 0$ and $x = 0.3$ at various temperatures are shown in Fig. 7.8. The coercive field values for each composition were found to exhibit an increase with decreased temperature. This is due to the influence of the metastable macro-domain structure and the immobilizations of the domain walls.[5]

The $x = 0.3$ and 0.5 compositions exhibited square loop behavior at -66°C. However, as the temperature increased the square loops transformed to slim loops and the remanent polarization and coercive filed values decreased significantly. *The* $x = 0$ and $x = 0.1$ compositions exhibited slim loop behavior near room temperature. All of compositions displayed a clear transition from square-loop behavior to slim-loop behavior in the vicinity of Tm. In addition, the hysteresis loops showed that the remanent polarization is non-zero at Tm but decays to zero at temperatures above Tm. Fig. 7.9 illustrates induced strain versus electric field at room temperature for compositions $x = 0.0 - 0.5$. The compositions low in PZT ($x = 0.0$-0.1) showed slim P-E loops indicating electrostrictive behavior; i.e. a second-order phenomenon of electromechanical coupling. With an increase PZT concentration micro-domain were observed to form. Fully formed loops were observed at the composition $x = 0.5$, indicated ferroelectric behavior. All compositions illustrate a clear transition from relaxor/electro-strictive behavior to normal ferroelectric behavior. These results are consistent with ferroelectric hysteresis loop and microstructural characteristics obtained from TEM.

7.3.4 TEM characterization

TEM examination provided supportive evidence for this phase transition sequence in the *0.5*PNN−*(1-x)*PZN−*x*PZT system. Fig. 7.10 illustrates the rhombohedral domain structures of 0.5PNN-0.5PZT: regular micron-sized domains were observed. When the PZT concentration decreased, the domain size decreased. The domain structures were decreased even further in size; nano-domain was observed at the composition $x = 0.0$ with profound relaxor characteristics. These results show the transition between micro-domain to nano-domain was observed with decrease in the normal ferroelectric PZT phase.

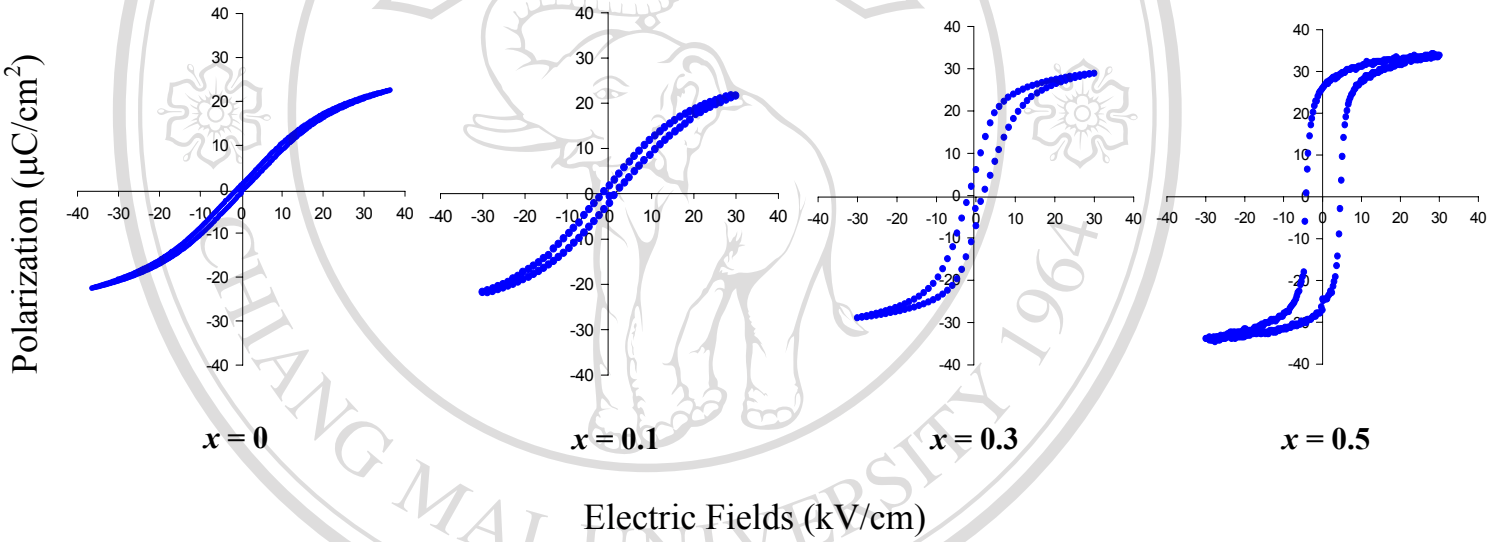

Figure 7.7 Room temperature polarization vs. electric field hysteresis loop of *0.5*PNN-(*0.5- x*)PZN-*x*PZT ceramic at the optimum sintering conditions.

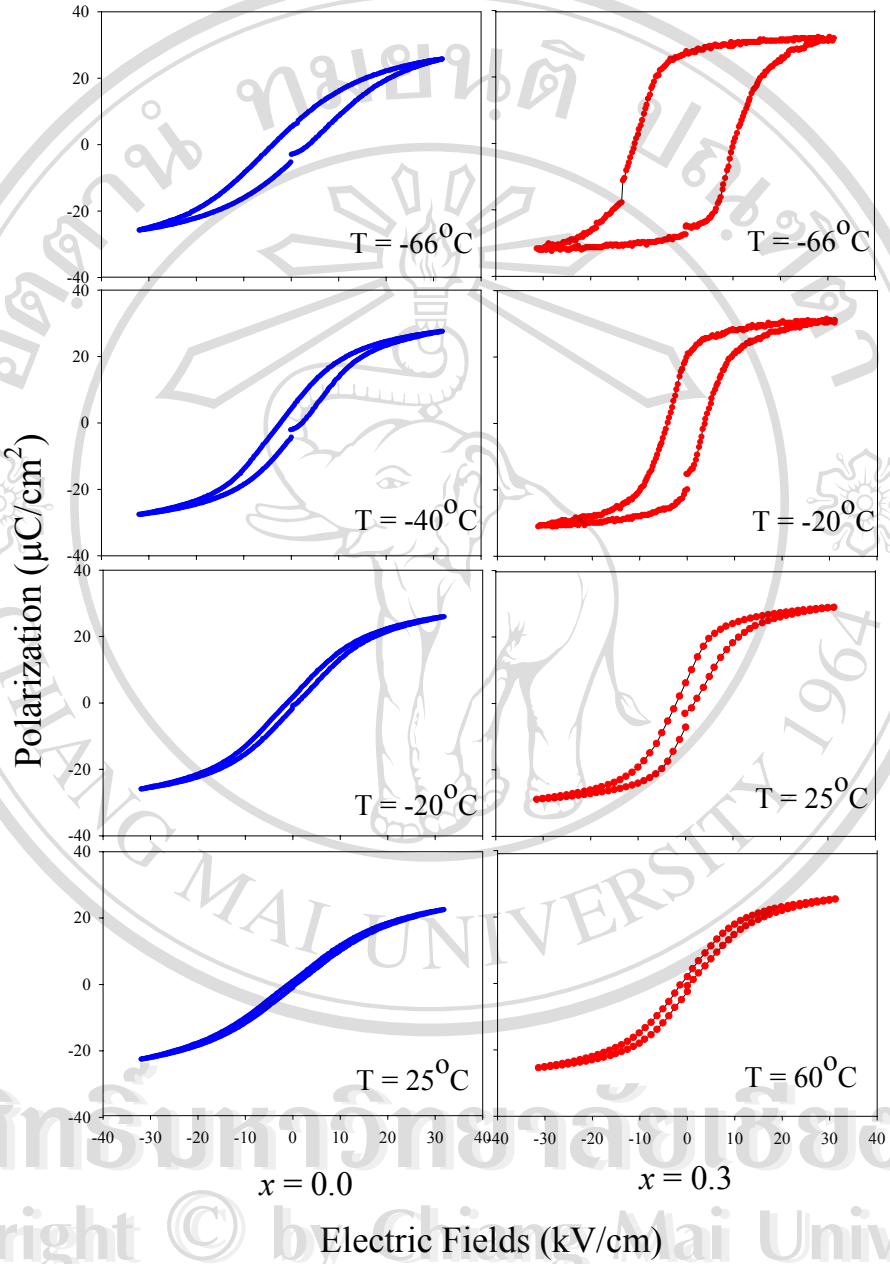

Figure 7.8 Temperature dependence of the $P-E$ hysteresis of *0.5*PNN–*(0.5-x)*PZN–*x*PZT ceramics at optimum sintering conditions, compositions $x = 0$ and $x = 0.3$ are shown.

Table 7.4 Polarization hysteresis data as a function of *x* in the *0.5*PNN–*(0.5-x)*PZN–*x*PZT system.

Composition	P_s (μC/cm^2)	P_r (μC/cm^2)	E_c (kV/cm)	Loop area (mC/cm^3)
x = 0.0	22.5	0.9	0.008	49.88
x = 0.1	23.8	1.8	0.010	72.81
x = 0.3	28.1	8.5	1.221	255.12
x = 0.5	31.9	25.2	4.024	628.47

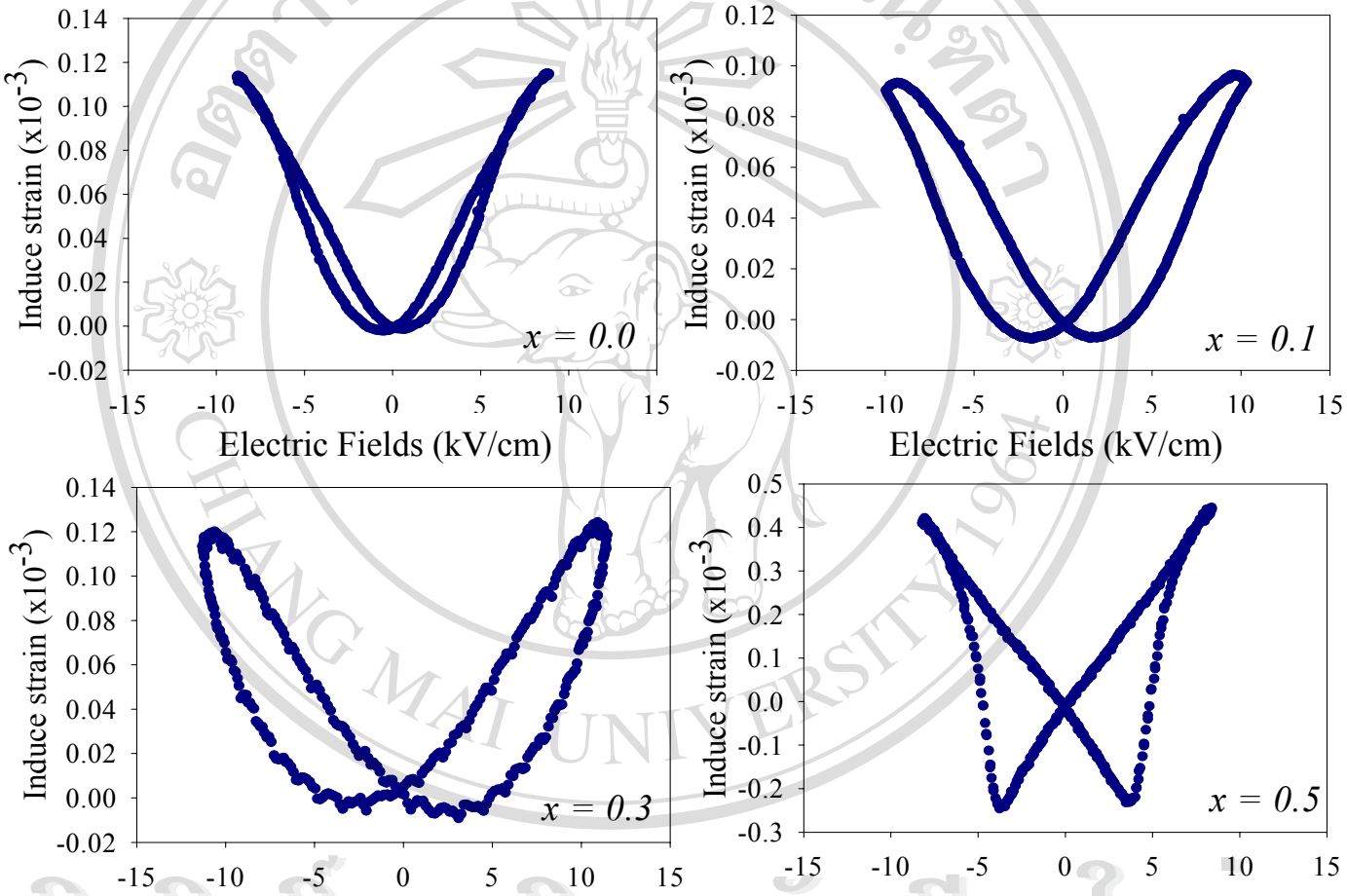

Figure 7.9 Induced strain vs. electric field butterfly loops for *0.5*PNN–*(0.5-x)*PZN–*x*PZT ceramics.

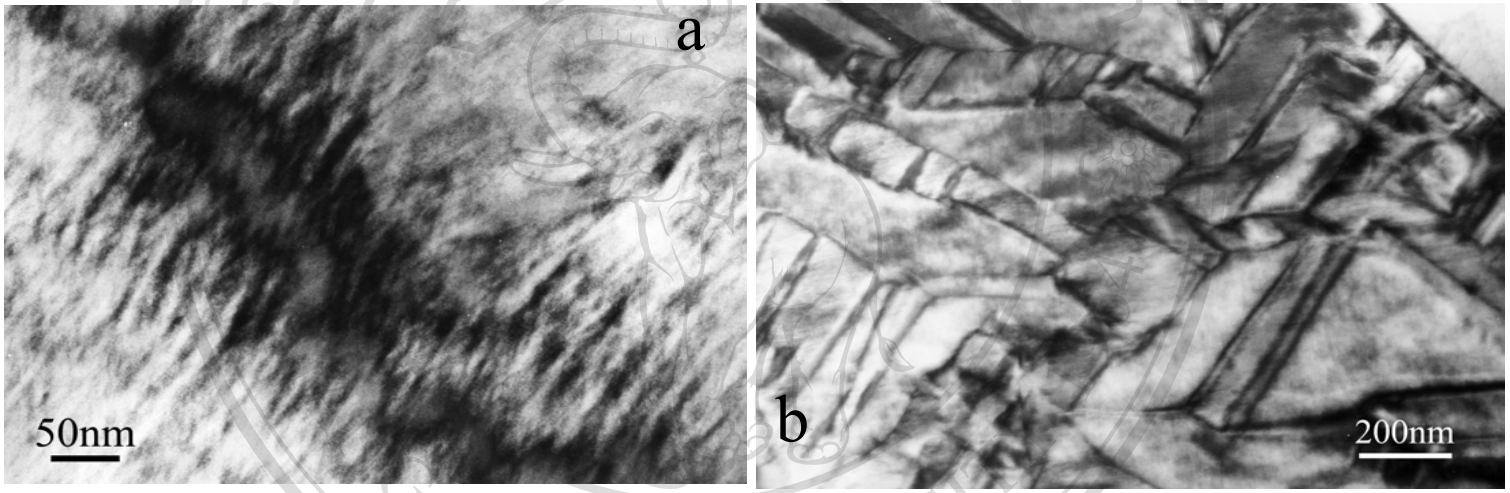

Figure 7.10 TEM micrographs of the *0.5*PNN-(*0.5-x*) PZN-*x*PZT ceramics; show the evolution of the micro-nano domain transition.(a) $x = 0.0$, showing nano-domain.(b) $x = 0.5$ showing micro-domain.

7.4 Conclustions

In this work, it was shown that by controlling PbO loss and preventing pyrochlore formation high permittivity ceramics in the PNN–PZN–PZT system can be processed through high temperature calcination. This can be accomplished by utilizing a double crucible during calcination, adding excess PbO (2mol%), and maintaining a fast heating/cooling rate (20^{o}C/min). The dielectric properties and the T_m of *0.5*PNN–*(0.5-x)*PZN–*x*PZT was found to increase with increasing PZT concentration. Furthermore the transition from the normal ferroelectric to the relaxor ferroelectric state was clearly observed as the mole fraction of PZT decreased. The optimum dielectric properties were observed for the $x = 0.5$ composition with a permittivity of 22,000 and P_s, P_r, and E_c values of 31.9 μC/cm^2, 25.2 μC/cm^2, and 4.0 kV/cm, respectively.